Published in final edited form as:
Structure. 2011 May 11; 19(5): 733–747. doi:10.1016/j.str.2011.02.009.

Structural and Energetic Determinants of Apo Calmodulin Binding to the IQ Motif of the $Na_v1.2$ Voltage-Dependent Sodium Channel

Michael D. Feldkamp[1], **Liping Yu**[1,2], and **Madeline A. Shea**[1,*]

[1] Department of Biochemistry Roy J. and Lucille A. Carver College of Medicine University of Iowa Iowa City, Iowa 52242-1109, USA

[2] NMR Facility Roy J. and Lucille A. Carver College of Medicine University of Iowa Iowa City, Iowa 52242-1109, USA

SUMMARY

The neuronal voltage-dependent sodium channel ($Na_v1.2$), essential for generation and propagation of action potentials, is regulated by calmodulin (CaM) binding to the IQ motif in its α-subunit. A peptide ($Na_v1.2_{IQp}$, KRKQEEVSAIVIQRAYRRYLLKQKVKK) representing the IQ motif had higher affinity for apo CaM than $(Ca^{2+})_4$-CaM. Association was mediated solely by the C-domain of CaM. A solution structure (2KXW.pdb) of apo $^{13}C,^{15}N$-CaM C-domain bound to $Na_v1.2_{IQp}$ was determined with NMR. The region of $Na_v1.2_{IQp}$ bound to CaM was helical; R1902, an $Na_v1.2$ residue implicated in familial autism, did not contact CaM. The apo C-domain of CaM in this complex shares features of the same domain bound to myosin V IQ motifs (2IX7) and bound to an SK channel peptide (1G4Y) that does not contain an IQ motif. Thermodynamic and structural studies of CaM-$Na_v1.2_{IQp}$ interactions show that apo and $(Ca^{2+})_4$-CaM adopt distinct conformations that both permit tight association with $Na_v1.2_{IQp}$ during gating.

Keywords

Allostery; NMR; Titration; Binding; Linkage; Solution Structure

INTRODUCTION

The voltage-dependent sodium channel type II ($Na_v1.2$) is required for propagation of action potentials along unmyelinated axons found primarily in neurons and muscle (Schaller and Caldwell, 2003). $Na_v1.2$ has one α-subunit and one or more β-subunits (Catterall, 2000). The α-subunit has four homologous, pore-forming transmembrane domains, and intracellular domains that control channel gating. Inactivation of $Na_v1.2$ α-subunit involves interactions of the intracellular loop connecting domains III and IV and the C-terminal tail which has been modeled to contain six α-helices (Cormier et al., 2002).

* To whom correspondence should be addressed. Telephone: (319) 335-7885. Fax: (319) 335-9570. madeline-shea@uiowa.edu .

Patch clamp studies showed that deletion of the putative sixth α-helix maintains the channel in a closed, inactivated state (Cormier et al., 2002; Mantegazza et al., 2001). A sequence (residues 1901 to 1927, $Na_v1.2_{IQp}$) within that region contains a classical CaM-binding IQ motif (Mori et al., 2000) (IQxxΦBGΦxxB), where X is any amino acid, Φ is an aromatic residue, and B is Arg or Lys (Figure 1A, B, C). All ten isoforms of Na_V contain a single IQ motif that allows channel regulation by CaM (Yu and Catterall, 2003). Many IQ motifs found in myosins, neuronal growth proteins, and ion channels bind preferentially to apo (Ca^{2+}-depleted) CaM (Liu and Storm, 1990; Urbauer et al., 1995). However, this preference is not universal. For example, the IQ motif in Ca_V 1.2 binds preferentially to $(Ca^{2+})_4$-CaM (DeMaria et al., 2001).

CaM is essential to many eukaryotic signal transduction pathways (Klee et al., 1986). As seen in Figure 1D, it is composed of two domains (N/blue and C/red) that each bind two Ca^{2+} ions cooperatively. Although the domains are similar in sequence and structure, the C-domain binds Ca^{2+} 10- to 25-fold more favorably than the N-domain (Klee et al., 1986). Ca^{2+} binding triggers opening of hydrophobic clefts in each domain of CaM, altering its free energy of association with target proteins (Crivici and Ikura, 1995). The canonical CaM-binding sequence forms a basic, amphipathic, alpha-helix (BAA motif) (Yap et al., 2000) that binds preferentially to $(Ca^{2+})_4$-CaM forming a compact ellipsoid (Figure 1E shows a BAA motif from CaMKII bound to $(Ca^{2+})_4$-CaM (1CDM)). There are few available structures of apo CaM bound to targets. In one, two apo CaM molecules are bound to a fragment of myosin V containing two IQ motifs (2IX7; (Houdusse et al., 2006), Figure 1F). The C-domain of CaM adopted a semi-open conformation having interhelical angles smaller than those of $(Ca^{2+})_4$-CaM. In another structure (1G4Y (Schumacher et al., 2001), Figure 1G), two CaM molecules, each having an apo semi-open C-domain but Ca^{2+}-saturated open N-domain, are bound to two copies of a fragment of the SK channel that does not contain an IQ motif. CaM is widely recognized for extreme molecular plasticity.

To understand the Ca^{2+}-dependent roles of each domain of CaM in binding the IQ motif of $Na_V1.2$, fluorescence spectroscopy and NMR were used to monitor thermodynamic and structural properties of association. We determined that the C-domain of CaM bound $Na_v1.2_{IQp}$ with very high affinity (nM K_d values), while the N-domain of CaM interacted weakly with the IQ motif. $Na_v1.2_{IQp}$ binding to CaM selectively reduced Ca^{2+}-binding affinity of sites III and IV, without significantly affecting sites I and II. Complexes of $Na_v1.2_{IQp}$ with apo CaM (the C-domain alone or full-length CaM) were unperturbed in the presence of elevated NaCl. Heteronuclear NMR studies of apo $^{13}C,^{15}N$-$CaM_{76\text{-}148}$ (C-domain alone) bound to $Na_v1.2_{IQp}$ were used to determine a solution structure. In it, the C-domain of CaM adopted a semi-open conformation in binding to the primarily helical peptide. Furthermore, although $Na_v1.2_{IQp}$ bound tightly to both apo and $(Ca^{2+})_4$-CaM, it caused unique chemical shift perturbations in each case. This suggests that the binding interface between $(Ca^{2+})_4$-CaM and $Na_v1.2_{IQp}$ is very different from that of apo $CaM_{76\text{-}148}$:$Na_v1.2_{IQp}$, consistent with the physiological function of Ca^{2+}-mediated inactivation $Na_v1.2$. These results are discussed with respect to CaM recognition of IQ motifs in general, and regulation of sodium channels specifically.

RESULTS

CaM Binding to $Na_v1.2_{IQp}$

CaM binding to fluoresceinated $Na_v1.2_{IQp}$ (Fl-$Na_v1.2_{IQp}$) was monitored by steady-state fluorescence emission to determine domain-specific differences in effects on peak intensity. As shown in Figure 2A for apo CaM, no change in Fl-$Na_v1.2_{IQp}$ was observed upon addition of 3 equivalents of $CaM_{1\text{-}80}$ (N-domain). Significant increases in intensity of Fl-$Na_v1.2_{IQp}$ were observed after addition of $CaM_{76\text{-}148}$ (C-domain, 15%) or $CaM_{1\text{-}148}$ (full-

length, 13%). This domain-specific pattern of change for apo CaM was preserved in 10 mM Ca^{2+} (Figure 2B), although the increase observed for $(Ca^{2+})_4$-CaM_{1-148} (25%) was larger than that for $(Ca^{2+})_2$-CaM_{76-148} (17%). The precision in intensity was ~1% for 3 replicate trials.

CaM Titration of $Na_v1.2_{IQp}$

The affinities of CaM binding to Fl-$Na_v1.2_{IQp}$ were determined using fluorescence anisotropy. Figure 2C shows that the anisotropy of Fl-$Na_v1.2_{IQp}$ increased upon binding either apo CaM (open symbols) or Ca^{2+}-saturated CaM (closed symbols). CaM_{1-80} bound to $Na_v1.2_{IQp}$ with low affinity (left panel); the K_d was 1.64 ± 0.65 μM for $(Ca^{2+})_2$-CaM_{1-80}, and 70.8 ± 5.7 μM for apo CaM_{1-80}. In contrast, both CaM1-148 and CaM_{76-148} (apo and Ca^{2+}-saturated forms) bound stoichiometrically to $Na_v1.2_{IQp}$, with a K_d ≤10 nM. The titrations were fit to a single-site binding isotherm that accounted for total CaM (Table S1); however, only an upper limit for the K_d can be determined under conditions of limiting CaM (Newman, 2008).

Effect of $Na_v1.2_{IQp}$ on Calcium Binding to CaM

To determine how $Na_v1.2_{IQp}$ affects the Ca^{2+}-binding properties of each domain of CaM, equilibrium titrations were performed on the isolated domains (CaM_{1-80}, CaM_{76-148}) and compared to the same sites within CaM_{1-148} (Figure 2D). Changes in intrinsic fluorescence intensity of phenylalanine reported on Ca^{2+} binding to sites I and II, while changes in tyrosine intensity reported on binding to sites III and IV. Total free energies of binding are listed in Table S2. Titrations are shown in blue (sites I and II) and red (sites III and IV) in the absence of peptide, and shown in cyan (sites I and II) and orange (sites III and IV) in the presence of peptide. Figure 2D shows that $Na_v1.2_{IQp}$ had little effect on sites I and II, whether in CaM_{1-80} (left panel) or CaM_{1-148} (right panel). However, it selectively reduced the Ca^{2+} binding affinity of sites III and IV of CaM_{76-148} (middle) by a factor > 500, and CaM_{1-148} (right) by a factor > 750 (Table S2).

Residue-Specific Effects of $Na_v1.2_{IQp}$ on CaM

Effects of $Na_v1.2_{IQp}$ on apo CaM were also manifested as conformational differences detected in the $^{15}N/^{1}H$-HSQC spectra. A spectral overlay of apo CaM_{1-148} alone and bound to $Na_v1.2_{IQp}$ showed that half of the observed amide chemical shifts were nearly identical (Figure S1). An overlay of $^{15}N/^{1}H$-HSQC spectra of apo CaM_{1-80} (N-domain) alone and apo CaM_{1-148} bound to $Na_v1.2_{IQp}$ (Figure S2) showed that resonances unperturbed by peptide binding were attributable to the N-domain. In contrast, resonances corresponding to C-domain residues were dramatically affected by peptide binding. Those in the spectrum of the apo CaM_{76-148}:$Na_v1.2_{IQp}$ complex were nearly identical to corresponding C-domain residues in apo CaM_{1-148}:$Na_v1.2_{IQp}$ (Figure S3). An overlay of three of these $^{15}N/^{1}H$-HSQC spectra in Figure 3A shows that the resonances of (a) apo CaM_{1-80} alone (green), and (b) apo CaM_{76-148} bound to $Na_v1.2_{IQp}$ (blue) closely resembled the spectrum of (c) apo CaM_{1-148} bound to $Na_v1.2_{IQp}$ (red).

Figure 3B shows the effect of Ca^{2+} binding. Almost all resonances in the ^{15} N-HSQC spectrum of $(Ca^{2+})_2$-CaM_{76-148} bound to $Na_v1.2_{IQp}$ (black) were distinct from those of apo CaM_{76-148} bound to $Na_v1.2_{IQp}$ (green), indicating that most backbone amides have different chemical environments, presumably because they have adopted distinct conformations.

Analysis of $^{15}N/^{1}H$-HSQC spectra of apo CaM_{76-148} ± $Na_v1.2_{IQp}$ (Figure 4A) showed that peptide binding caused significant chemical shift perturbations (Δδ) of the CaM backbone amides ($\delta_{average}$ of 0.51 ppm). It also dramatically increased dispersion of $^{15}N/^{1}H$-HSQC cross peaks (Figure 4A) by breaking the symmetry of similar chemical environments of

homologous residues in the paired EF-hands of apo $CaM_{76\text{-}148}$. Mapping Δδ onto the sequence of $CaM_{76\text{-}148}$ (Figure 4B) indicated that the greatest perturbations were observed in the region between helices F and G. For residues 108-117,$\Delta\delta_{average}$ was 1.47 ppm. Unassigned amides (for residues 76, 132, 133, 134, 135, and 141) are indicated with short gray bars below the abscissa; yellow bars indicate Ca^{2+}-binding sites III and IV.

Hydrogen/Deuterium Backbone Amide Exchange

Backbone amide hydrogen/deuterium exchange rates of apo $CaM_{76\text{-}148}$:$Na_v1.2_{IQp}$ were determined to identify slowly exchanging amides that are usually located in regions of persistent secondary structure. In the $^{15}N/^{1}H$-HSQC spectrum, 37 amide resonances were detected 30' after addition of D_2O to a lyophilized sample. Protection factors (Table S3) were calculated from the decay of cross peak intensities (examples shown in Figure 4C) that were fit to a mono-exponential function (Figure 4D) and corrected for intrinsic exchange rates (Figure 4E) (Bai et al., 1993; Molday et al., 1972). Residues with observable exchange rates were used as H-bond restraints during subsequent structure calculations.

Structure of Apo $CaM_{76\text{-}148}$:$Na_v1.2_{IQp}$

Structural statistics of the apo $CaM_{76\text{-}148}$:$Na_v1.2_{IQp}$ complex are in Table 1. This structure was determined based on 109 dihedral angular restraints and 1865 unambiguous distance restraints comprised of 457 intra-residue, 298 short, 300 medium, 331 long, 245 intra-peptide, 188 intermolecular, and 46 hydrogen bonds. The restraints are distributed evenly throughout the protein, with a slightly higher number observed in α-helical and β-sheet regions than in the empty Ca^{2+}-binding sites III and IV. Figure 5A shows a superposition of the 20 lowest energy structures of the apo $CaM_{76\text{-}148}$:$Na_v1.2_{IQp}$ complex that best satisfied the experimental restraints. The interhelical angles calculated by UCSF Chimera (Pettersen et al., 2004) between helices E-F and G-H of these structures were 77.4° ± 1.7 and 78.0° ± 2.3 respectively. The apo $CaM_{76\text{-}148}$:$Na_v1.2_{IQp}$ complex was well defined, with an ensemble RMSD of 0.31 ± 0.05 Å (Table 1). Figure S4 shows a Ramachandran plot of the final averaged structure.

Interface Between $Na_v1.2_{IQp}$ and Apo $CaM_{76\text{-}148}$

The hydrophobic interface of apo $CaM_{76\text{-}148}$:$Na_v1.2_{IQp}$ was well defined as judged by the constrained positions of interacting residues (Figure 5B). The buried solvent-accessible hydrophobic surface calculated using GETAREA (Fraczkiewicz and Braun, 1998) was 1393 $Å^2$ (751 $Å^2$ $Na_v1.2_{IQp}$, 642 $Å^2$ apo $CaM_{76\text{-}148}$). In apo $CaM_{76\text{-}148}$, hydrophobic residues A88, V91, F92, L112, and M145 accounted for 43% of its buried surface, while in $Na_v1.2_{IQp}$, hydrophobic residues V1911, I1912, Y1916, Y1919, and L1920 accounted for 53.5% of its buried surface area. To demonstrate how well residues at the interface were constrained, a superposition of the 20 lowest energy structures was rotated by 2° increments in PyMol and captured with ImageJ. Movie S1 shows an overlay of apo $CaM_{76\text{-}148}$ models (wireframe) bound to $Na_v1.2_{IQp}$ (cartoon and sticks). Movie S2 shows the apo $CaM_{76\text{-}148}$ models with all sidechains, followed by models showing only hydrophobic sidechains located at the interface with $Na_v1.2_{IQp}$.

Figure 5C shows vacuum electrostatic potentials for coordinates of apo $CaM_{76\text{-}148}$ and $Na_v1.2_{IQp}$ corresponding to their conformation in the complex as calculated using Pymol (Schrödinger, LLC.). As expected, favorable electrostatic interactions were observed between negatively charged apo $CaM_{76\text{-}148}$ and positively charged $Na_v1.2_{IQp}$., and the interface is dominated by hydrophobic surface.

Figure 6A shows all contacts between apo $CaM_{76\text{-}148}$ and $Na_v1.2_{IQp}$ that are • 4.5 Å (tabulated by by *Contacts of Structural Units (CSU)* (Sobolev et al., 1999)). Interactions of

the IQ residues (I1912, Q1913) with apo CaM_{76-148} were identified on the basis of numerous NOEs detected in (a) the 3D ^{13}C-edited and ^{15}N-edited NOESY spectra and (b) the ^{13}C-edited and ^{12}C,^{14}N-filtered 3D NOESY spectra. Figures 6B and 6C show NOEs for selected residues of apo CaM_{76-148}. As seen in the CSU analysis, I1912 inserted into the shallow hydrophobic pocket of semi-open apo CaM_{76-148} (Figure 6D) while Q1913 formed hydrogen bonds with backbone atoms L112 and E114 in the turn connecting helices F and G (Figure 6E). A comparison of CaM sequences from 102 species (Ataman et al., 2007) showed that residues E114 and G113 were identical in all, while L112 was 89.2% identical.

Calcium Binding to Apo CaM_{1-148}:$Na_v1.2_{IQp}$ Complex

Figure 7A shows that apo CaM_{1-148} bound to $Na_v1.2_{IQp}$ underwent a structural transition upon Ca^{2+} binding. Figure 7A (left panel) shows the overlay of $^{15}N/^{1}H$-HSQC spectra of apo CaM_{1-148} (red) and $(Ca^{2+})_4$-CaM_{1-148} (black) bound to $Na_v1.2_{IQp}$, indicating that Ca^{2+} caused significant change in the chemical environment of apo CaM_{1-148} resonances within the complex. For reference, Figure 7A (right panel) compares $(Ca^{2+})_4$-CaM_{1-148} alone and after addition of $Na_v1.2_{IQp}$. Figures 7B, C, and D show the $^{15}N/^{1}H$-HSQC cross peaks for selected residues of the N- and C-domains of apo CaM_{1-148} when bound to $Na_v1.2_{IQp}$ at increasing [Ca^{2+}]. The N-domain of apo CaM_{1-148} was in fast exchange over the course of the Ca^{2+} titration; representative resonances are shown in Figure 7B. Plots of the normalized Ca^{2+}-dependent change in chemical shifts indicated that the N-domain titrated almost completely between 0 and 2 Ca^{2+} equivalents.

Observation of Ca^{2+}-induced changes in peak position and intensity of the C-domain of apo CaM_{1-148} bound to $Na_v1.2_{IQp}$ (Figure 7C) showed that peaks were in intermediate or slow exchange. Thus, changes in peak intensities were used to determine relative populations over the course of the titration. These peaks broadened beyond the limit of detection after addition of 2 equivalents of Ca^{2+} (Figure 7C) as has been seen for Ca^{2+} binding to melittin-bound CaM (Newman, 2008). New peaks that appeared at the midpoint of the Ca^{2+} titration and increased through the addition of 4 equivalents of Ca^{2+} (see Figure 7D) are likely to correspond to residues in the C-domain of $(Ca^{2+})_4$-CaM_{1-148} based on correlations with effects of $Na_v1.2_{IQp}$ on Ca^{2+}-binding shown in Figure 2. These data indicated that, when bound to $Na_v1.2_{IQp}$, each domain of CaM_{1-148} binds 2 Ca^{2+}, and sites I and II have a slightly more favorable Ca^{2+}-binding affinity than sites III and IV.

Effect of Ca^{2+} on CaM_{1-148}:$Na_v1.2_{IQp}$

As shown in Figure 2C, apo CaM_{1-148} bound to Fl-$Na_v1.2_{IQp}$ stoichiometrically at a 1:1 ratio, with binding mediated by the C-domain of CaM. If Ca^{2+} binding to CaM_{1-148} induced association of the N-domain with $Na_v1.2_{IQp}$, then the structure would become more compact. To test this, Ca^{2+} was added to apo CaM_{1-148}:Fl-$Na_v1.2_{IQp}$ (Figure S5A). The hydrodynamic behavior of the complex was monitored by fluorescence anisotropy, but no change was observed. Evaluated with the NMR spectra in Figures 3 and 7, this suggests that the Ca^{2+}-saturated N-domain is free to bind elsewhere on $Na_v1.2$ or to another target protein.

Effect of Na^+ upon $Na_v1.2_{IQp}$ Binding to CaM

Proteins in the plasma membrane experience large fluctuations in Na^+ concentration during $Na_v1.2$ gating (Venosa, 1974) which might affect the affinity of $Na_v1.2_{IQp}$ for CaM. To test this, Fl-$Na_v1.2_{IQp}$ was saturated with apo CaM_{76-148} or apo CaM_{1-148} and then titrated with NaCl in a matching buffer over a range from 0 to 650 mM (Figure S5B). The observed anisotropy of $Na_v1.2_{IQp}$ was constant, indicating that NaCl has a negligible effect on $Na_v1.2_{IQp}$ dissociation from CaM.

DISCUSSION

$Na_v1.2$ contains a CaM-binding IQ motif involved in channel inactivation which is necessary for controlling Na^+ balance. Thermodynamic studies and the structure of apo semi-open $CaM_{76\text{-}148}$ bound to $Na_v1.2_{IQp}$ reported here provide insights regarding the roles of residues that are conserved in IQ motifs in ion channels, and differences between the two domains of CaM. They provides a foundation for further studies of Ca^{2+}-mediated switching of channel activity.

Domain-Specific Binding of CaM to $Na_v1.2_{IQp}$

The energetics of CaM binding to $Na_v1.2_{IQp}$ reflect large differences between the two domains of CaM that would permit major regulatory differences. In the complex, apo $CaM_{76\text{-}148}$ did not contact R1902, a residue implicated in familial autism (R1902C is known to interfere with binding of $(Ca^{2+})_4$-CaM (Weiss et al., 2003)). This leaves open the question of how $(Ca^{2+})_2$-$CaM_{76\text{-}148}$ interacts with R1902, and whether the mutation may exert its influence via effects on the tertiary structure of the channel. The CaM C-domain is necessary and sufficient for binding $Na_v1.2_{IQp}$. Its high affinity (nM K_d) for CaM would promote constitutive binding to $Na_v1.2$ independent of intracellular $[Ca^{2+}]$. Strong, Ca^{2+}-independent binding is similar to behavior observed for $Na_v1.4$ in electrophysiological and FRET studies by Tomaselli and coworkers who showed that CaM remained bound to the IQ motif region as $Na_v1.4$ adopted multiple conformations in response to voltage changes and Ca^{2+} (Biswas et al., 2008). The weak (μM) affinity of $CaM_{1\text{-}80}$ for $Na_v1.2_{IQp}$ and residue-specific NMR studies showing that $Na_v1.2_{IQp}$ caused barely detectable perturbations of the N-domain (either as a fragment or within full-length CaM) both argue that the N-domain of CaM does not bind $Na_v1.2_{IQp}$ in a manner that is physiologically significant.

Effect of $Na_v1.2_{IQp}$ on Ca^{2+} Binding

Unlike kinases that increase the Ca^{2+}-binding affinity of both domains of CaM by interacting favorably with the open conformation of each domain, binding of $Na_v1.2_{IQp}$ selectively lowered the overall Ca^{2+}-binding affinity of CaM by 4.03 kcal/mol (Figure 2D). This decrease was attributable almost entirely to interactions of the C-domain of CaM ($\bullet\bullet G_2$ of 3.89 kcal/mol; Table S1). Binding of $Na_v1.2_{IQp}$ imposed tertiary constraints that lowered the probability of Ca^{2+} binding to sites III and IV. The effects of $Na_v1.2_{IQp}$ on $\bullet G_2$ for Ca^{2+} binding to the individual domains of CaM was additive (i.e., similar that observed in $CaM_{1\text{-}148}$), indicating that interdomain interactions in $CaM_{1\text{-}148}$ were minimal (Table S1). This was consistent with domain-specific effects seen with fluorescence in Figure 2A, B, C and with NMR in **Figures** 3, S1, S2, and S3.

Semi-Open Apo C-domain Binds IQ Motifs

Figure 8A shows a structural comparison of (a) apo $CaM_{76\text{-}148}$ bound to $Na_v1.2_{IQp}$ (determined in this study) to (b) the C-domains of two apo $CaM_{1\text{-}148}$ molecules bound to two neighboring IQ motifs found in myosin V (2IX7), (c) apo CaM-like proteins bound to IQ motifs of MYO2P (1M46, 1M45, 1N2D) and (d) ELC bound to myosin heavy chain (3JVT). In all of these, each set of paired EF-hands of the C-domain adopts a semi-open conformation when bound to its respective IQ motif. Moreover, the residues located at positions “0”/Ile and “1”/Gln of the IQ motif interact with a similar subset of residues in the apo C-domain.

At position “0”, a hydrophobic (typically branched) residue contacts hydrophobic sidechains of the semi-open C-domain, burying what would otherwise be solvent-exposed hydrophobic surface. Conservation of Gln at position “1” of canonical IQ motifs preserves hydrogen bonding interactions between its carboxamide and the backbone of CaM residues located in

the turn connecting α-helices F and G (Figure 6E). As observed in the $^{15}N/^{1}H$-HSQC data (Figure 4A and 4D), residues located in this turn exhibited the largest chemical shift perturbation upon peptide binding. Examination of amide hydrogen exchange protection factors mapped onto the structure (Figure 4F) suggests that this turn is solvent-exposed. Therefore, the H-bonds involved in this turn may be different from those observed in classic α-helices and β-sheets.

Tomaselli and coworkers, studying $Na_V1.4$, showed that residues I and Q are required for gating, and that substitution by alanine eliminated the proximity of CaM to the C-terminus of $Na_v1.4$ under all conditions (e.g., resting and high Ca^{2+}) (Biswas et al., 2008). The interactions observed between the IQ residues of $Na_v1.2_{IQp}$ and apo CaM could not be satisfied by alanine substitutions. With Ala at position "0", there would be less of a penalty for solvent exposure relative to Ile, Leu, Met, or Phe at that position. With Ala at position "1", there would be no carboxamide interaction between the sodium channel and atoms in the backbone of the loop between α-helices F and G of CaM.

Semi-Open Apo C-Domain Binding to a Non-IQ motif

An apo domain of CaM can bind to a sequence without an IQ motif, as seen in the 1G4Y structure of partially apo CaM bound to a peptide (SK_p, gating domain residues 413-488) derived from the small conductance potassium channel (SK Channel) (Schumacher et al., 2001). A superposition of apo $CaM_{76\text{-}148}$:$Na_v1.2_{IQp}$ and the apo C-domain of 1G4Y showed that both adopt the semi-open conformation (Figure 8B).

SK_p shares a key feature seen in the IQ motif-containing peptides bound to apo CaM, CaM-like proteins, and ELC. Figures 8A and 8B show that a carboxamide-containing side chain (Asn in SK_p vs. Gln in IQ motifs) forms hydrogen bonds with backbone residues between the F and G helices of CaM. This conserved hydrogen-bonding network influences the position of the IQ motif or SK_p helix relative to the apo C-domain. Another similarity was apparent in the conserved hydrophobic interaction between I1912 ($Na_v1.2_{IQp}$) or L428 (SK_p) and the core of the apo C-domain (Figure 8B), even though these residues differ in their position in the primary sequence relative to the carboxamide side chain (Q1913 in $Na_v1.2_{IQp}$ or N426 in SK_p).

As depicted in Figure 8C, both SK_p and $Na_v1.2_{IQp}$ adopted the $_{N}F\text{-}G_{C}$ orientation. where F and G refer to the helices of CaM between sites III and IV, and N and C refer to the termini of the CaM-binding sequence. In $Na_v1.2_{IQp}$, the conserved hydrophobic residue (I1912) that inserts into the core of apo $CaM_{76\text{-}148}$ precedes the conserved carboxamide-containing residue (Q1913). Although in SK_p, L428 (the residue homologous to I1912) is located 2 residues distal to the carboxamide-containing residue (N426), the relative angular positions of IQ and N-L are the same (Figure 8D). This illustrates how peptides can recognize the semi-open conformation of apo C-domain regardless of whether they contain an IQ motif.

Orientations of IQ motif Binding to CaM

If the contacts seen in Figure 8A were maintained by all apo CaM-binding motifs, then all canonical IQ motifs would bind to the semi-open C-domain of apo CaM in the $_{N}F\text{-}G_{C}$ orientation. At this time, there are too few deposited structures of apo CaM bound to IQ motifs to test this prediction. Figure 9 (upper panel) depicts available structures of apo CaM and $(Ca^{2+})_4$-CaM bound to peptides containing canonical IQ motifs derived from indicated target proteins. In these cases, position "0" is occupied by Ile in all structures except that of myosin V^B (which has Val), and position "1" is only occupied by Gln. The orientation of peptide binding to each of this is $_{N}F\text{-}G_{C}$ (N- and C- termini of peptide blue and magenta respectively), as depicted by rightward arrows.

We infer that apo CaM binds to $Na_v1.2_{IQp}$ and other canonical IQ motifs in the $_NF\text{-}G_C$ orientation because of the Gln located at position "1". The simplest model for Ca^{2+}-mediated regulation of $Na_V1.2$ is that the $_NF\text{-}G_C$ orientation is also used by $(Ca^{2+})_4$-CaM when binding $Na_v1.2$, because $_NF\text{-}G_C$ has been observed in all structures of $(Ca^{2+})_4$-CaM bound to canonical IQ-motifs from other channels. Adoption of the opposite ($_CF\text{-}G_N$) orientation by $(Ca^{2+})_4$-CaM would require the C-domain of apo CaM to release from the IQ motif upon Ca^{2+} influx, and re-associate when Ca^{2+}-saturated.

Both orientations of $(Ca^{2+})_4$-CaM have been observed (Figure 9, lower panel) in complexes with peptides that contain non-canonical IQ motifs (e.g., sequences having Met or Phe at position "1", rather than Gln). Structures of $(Ca^{2+})_4$-CaM bound to fragments with these sites from $Ca_v2.1$, $Ca_v2.2$, and $Ca_v2.3$ adopted alternative orientations in different studies. Different peptide lengths of $Ca_v2.1$ and $Ca_v2.3$, and distinct crystallization conditions were used in these studies, which may account for the structural differences (Kim et al., 2008; Mori et al., 2008). At this time, there are no available structures of apo CaM bound to a Ca_V IQ-motif.

Role of the N-domain of $CaM_{1\text{-}148}$ in $Na_v1.2$ Recognition

The N-domains of both apo and $(Ca^{2+})_4$-$CaM_{1\text{-}148}$ do not interact with $Na_v1.2_{IQp}$ as shown by titrations monitored by steady-state fluorescence (Figures 2A and 2B), fluorescence anisotropy (Figure 2C), and additive $^{15}N/^{1}H$-HSQC spectra (**Figures** 3A, S2). However, studies presented here do not rule out that it may interact elsewhere on $Na_V1.2$, as suggested schematically in Figure 8E by site X (for the apo closed N-domain) and site Y (for the Ca^{2+}-saturated open N-domain). The interaction of apo N-domain might mimic that seen in a complex of CaM bound to a fragment of the anthrax edema factor (Drum et al., 2002) which involves a helix-helix interaction rather than an interface with the cleft of CaM.

Previous studies (Mori et al., 2000) showed that $Na_v1.2$ contains a second CaM-binding motif comprised of residues 1913-1938 ($Na_v1.2_{BAA\text{-}1913\text{-}1938}$) that binds to $(Ca^{2+})_4$-CaM, but not apo CaM. This sequence has characteristics of a classic BAA-motif that preferentially binds the open conformation of Ca^{2+}-saturated CaM. Thus, the N-domain could bind to a site within $Na_v1.2_{1913\text{-}1938}$ while the C-domain remains tethered to $Na_v1.2_{IQp}$ (Figure 8E). To test this model, Fl-$Na_v1.2_{IQp}$ was titrated with apo $CaM_{1\text{-}148}$ and monitored by fluorescence anisotropy (Figure S6A) to assure saturation. When $Na_v1.2_{1913\text{-}1938}$ was added in 6-fold excess, it competed for $Na_v1.2_{IQp}$; there was no evidence for simultaneous binding of both $Na_v1.2$ 2_{IQp} and $Na_v1.2_{1913\text{-}1938}$ to $(Ca^{2+})_4$-CaM. This suggests that a binding site for Ca^{2+}-saturated N-domain may be located elsewhere in $Na_v1.2$ or another protein (shown schematically as site Y in Figure 8E). For example, the intracellular linker between domains III and IV of other sodium channels binds $(Ca^{2+})_4$-CaM (Sarhan et al., 2009; Shah et al., 2006). Alternatively, the conformation of these residues within $Na_v1.2$ may not be fully represented by a peptide.

Conclusion

The studies reported here provide the first structure of apo $CaM_{76\text{-}148}$:$Na_v1.2_{IQp}$. The structural interface and the binding energy for association of $Na_v1.2_{IQp}$ and apo CaM are mediated by the C-domain alone. This implies that a preferred binding site for the N-domain of CaM must lie elsewhere. In the apo $CaM_{76\text{-}148}$:$Na_v1.2_{IQp}$ structure, CaM adopts a semi-open conformation similar to the C-domain of apo CaM alone (Swindells and Ikura, 1996), CaM-like proteins (Terrak et al., 2003), essential light chain (ELC) (Swindells and Ikura, 1996), apo CaM when bound to IQ motifs in myosin (Houdusse et al., 2006) and the apo C-domain of CaM bound to the SK channel (Schumacher et al., 2001). At the CaM-peptide interface in apo $CaM_{76\text{-}148}$:$Na_v1.2_{IQp}$, the highest number of noncovalent interactions was

observed between apo CaM_{76-148} and 4 residues (I1912, Q1913, Y1916, and Y1919) of $Na_v1.2_{IQp}$. These sidechains are strongly conserved in IQ motifs found in Na_V isoforms, with the exception of the Y1919 which is a histidine in four of the ten isoforms (Figure 1A). There are now multiple structures of $(Ca^{2+})_4$-CaM bound to peptides representing IQ motifs of ion channels, but there are no cases in which the corresponding complex of apo CaM bound to the same peptide is available. Discovering how Ca^{2+}-mediated switching of CaM regulates $Na_V1.2$ will require future analysis of calcium-saturated CaM_{76-148}:$Na_v1.2_{IQp}$, studies of apo CaM binding to $Na_v1.2_{IQp}$ having substitutions that mimic mutations known to alter gating properties, and dissection of interactions of CaM with larger fragments of the intracellular C-terminal sequence of the channel.

EXPERIMENTAL PROCEDURES

Calmodulin

Isotopes were obtained from Cambridge Isotope Laboratories (Andover, MA). CaM over-expression was IPTG-induced in *E. coli* BL21(DE3) cells containing a recombinant pT7-7 vector expressing full-length (residues 1-148), N-domain (1-80), or C-domain (76-148) of *Paramecium* CaM (C. Kung, University of Wisconsin, Madison, WI) which is 88% identical to mammalian CaM. A genetic screen of *Paramecia* demonstrated that CaM mutations directly affected Na^+ channel function and chemotactic behavior (Kung et al., 1992). ^{15}N-labeled proteins were over-expressed in minimal media (2 g/L unlabeled glucose as carbon source, 1 g/L $^{15}NH_4Cl$ as sole nitrogen source). ^{13}C,^{15}N-labeled proteins were produced using 2 g/L ^{13}C-glucose as sole carbon source and 1 g/L $^{15}NH_4Cl$ as sole nitrogen source. CaM was purified as described previously (Putkey et al., 1985). Proteins were 97-99% pure as judged by silver-stained SDS-PAGE gels; concentration was determined by UV spectroscopy of CaM native at pH 7.4 or denatured with NaOH.

Peptides

GenScript Corporation (Scotch Plains, NJ) synthesized peptides representing residues 1901-1927 of the $Na_v1.2$ α-subunit (KRKQEEVSAIVIQRAYRRYLLKQKVKK, 3.36 kDa) with (Fl-$Nav1.2_{IQp}$) or without ($Nav1.2_{IQp}$) fluorescein at the N-terminus. The W.M. Keck Biotechnology Resource Center (New Haven, CT) synthesized $Na_v1.2_{BAA-1913-1938}$ representing residues 1913 to 1938 of the $Na_v1.2$ α-subunit (QRAYRRYLLKQKVKKVSSIYKKDKGK).

Emission Spectra

Emission spectra (λ_{ex} 430 nm, bandpasses 2 nm (excitation), 10 nm (emission)) of Fl-$Na_v1.2_{IQp}$ (1 μM) ± 3 μM CaM_{1-148}, CaM_{1-80} or CaM_{76-148} in 50 mM HEPES, 100 mM KCl, 5 mM NTA, 50 μM EGTA, and 1 mM $MgCl_2$ (pH 7.4) were collected at 22 °C with a PTI-QM4 Fluorimeter (PTI, Birmingham, NJ). Apo samples were Ca^{2+}-saturated by addition of $CaCl_2$ in matching buffer to a final concentration of 10 mM. Spectra were normalized to λ_{max} of Fl-$Na_v1.2_{IQp}$ alone and corrected for dilution.

Equilibrium Calcium Titrations

Ca^{2+} titrations of sites I and II (N-domain) and sites III and IV (C-domain) of CaM alone (6 μM) or with 9 μM $Na_v1.2_{IQp}$ (50% excess) were monitored at 22 °C with a PTI-QM4 Fluorimeter (Photon Technology International, Birmingham, NJ) and analyzed as described previously (Theoharis et al., 2008).

$Na_v1.2_{IQp}$ Titration of CaM_{1-148}

$^{15}N/^{1}H$-HSQC spectroscopy monitored a titration of $Na_v1.2_{IQp}$ into apo ^{15}N-CaM_{1-148} (400 μM) in 10 mM D_4-imidazole, 100 mM KCl, 50 μM D_{16}-EDTA, 0.01% NaN_3, pH 6.8. Upon saturation of apo CaM_{1-148} with $Na_v1.2_{IQp}$, $CaCl_2$ was added to a final concentration of 5 mM. $Na_v1.2_{IQp}$ and Ca^{2+} saturation of CaM_{1-148} were confirmed by plateaus in the intensity of peaks corresponding to either the $Na_v1.2_{IQp}$:apo CaM_{1-148} or $Na_v1.2_{IQp}$:$(Ca^{2+})_4$-CaM_{1-148}.

Preparation of $^{13}C,^{15}N$-CaM_{76-148}:$Na_v1.2_{IQp}$ Complex

A 1.5 mM 1:1 complex of $^{12}C,^{14}N$-Na 1.2_{IQp}:^{13}C, ^{15}N-apo CaM_{76-148} was prepared in 10 mM D_4-imidazole, 100 mM KCl, 50 μM D_{16}-EDTA, 0.01% NaN_3, pH 6.8. Nitrogen-based experiments were conducted in 90% H_20 / 10% D_20, while carbon-based experiments were conducted in 100% D_2O. All spectra, with the exception of amide exchange, were collected on samples in Shigemi (Allison Park, PA) microscale NMR tubes whose magnetic susceptibility was matched to D_2O.

$^{15}N/^{1}H$-HSQC Monitored Amide Exchange of ^{15}N-CaM_{76-148}:$Nav1.2_{IQp}$ Complex

The $^{12}C,^{14}N$-$Na_v1.2_{IQp}$:^{13}C, ^{15}N-apo CaM_{76-148} complex (described above) was lyophilized in a Speed-Vac Model VG-5 (Savant). The complex was re-suspended in 99.96% D_2O (Cambridge Isotope Laboratories, Andover, MA). HMQC spectra prior to lyophilization in H_2O were identical to those taken in D_2O. The pH of the sample was not adjusted after addition of D_2O. The sample was placed immediately in a Bruker 500 MHz Avance II spectrometer; data acquisition began within 5 min. $^{15}N/^{1}H$-HSQC spectra were acquired at intervals of 30 min for 23 h. Spectra were processed with NMRPipe (Delaglio et al., 1995). Individual peak intensities were determined with Sparky (Goddard and Kneller). Using the Solver function in Microsoft Excel, peak intensities were fit to Equation 1.

$$I=I_0e^{-(t-t_0)/\tau}+b \tag{1}$$

where I is intensity at time t, I_0 is initial intensity, t_0 is time zero, τ is the apparent decay lifetime, and b represents intensity at the asymptote.

Structure Determination

NMR spectra were collected at 25 °C on either a Bruker Avance II 500 MHz or cryoprobe-equipped 800 MHz spectrometer. The ^{1}H, ^{15}N, and ^{13}C resonances of the apo CaM_{76-148} backbone were assigned using triple resonance experiments (HNCA, HN(CO)CA, HNCACB, HN(CO)CACB, HNCO, and HN(CA)CO) (Yamazaki et al., 1994) with uniformly $^{13}C,^{15}N$-labeled apo CaM_{76-148} bound to unlabeled $Na_v1.2_{IQp}$. $^{1}H_\alpha$ resonances were assigned from an ^{15}N-edited TOCSY spectrum using a uniformly ^{15}N-labeled protein (Clore and Gronenborn, 1994) and from HA(CACO)NH experiments using a uniformly ^{15}N and ^{13}C-labeled sample. Side chains were assigned from 3D H(CCO)NH-TOCSY, C(CO)NH-TOCSY, HCCH-TOCSY, ^{15}N-edited TOCSY, and ^{15}N or ^{13}C edited NOESY spectra (Clore and Gronenborn, 1994; Fesik and Zuiderweg, 1988).

CaM was ^{13}C, ^{15}N-labeled but $Na_v1.2_{IQp}$ had natural abundance isotopes. We used isotope-filtered 2D TOCSY and NOESY experiments with mixing times of 26 to 46 ms (Gemmecker et al., 1992; Ikura and Bax, 1992; Otting and Wuthrich, 1989) to assign the unlabeled $Na_v1.2_{IQp}$. Isotope-filters for ^{13}C and ^{15}N were employed twice (once preceding t_1 and once preceding t_2) to effectively suppress the signals derived from ^{13}C-attached protons and ^{15}N-attached protons. As a result, 2D spectra for protons located on the unlabeled peptide were obtained; thus, only intrapeptide signals were observed in these

doubly isotope-filtered spectra. To assign intermolecular NOEs between the unlabeled peptide and $^{13}C,^{15}N$-CaM, we used ^{13}C-edited and $^{14}N,^{12}C$-filtered 3D NOESY experiments with mixing times of 80 to 120 ms as described previously (Burgering et al., 1993). Representative intrapeptide and intermolecular NOEs of the CaM/peptide complex were shown in Figure 6. All spectra were processed with NMRPipe (Delaglio et al., 1995) and analyzed with Sparky (Goddard and Kneller).

Apo $CaM_{76\text{-}148}$:$Na_v1.2_{IQp}$ Structure Calculations

Structures of the complex were generated using a torsion-angle molecular dynamics protocol (Stein et al., 1997) with CNS (Brunger et al., 1998). Structure calculations employed 1819 NMR-derived distance restraints from the analysis of 3D ^{15}N- and ^{13}C-resolved NOESY spectra acquired with a mixing time of 120 ms (Fesik and Zuiderweg, 1988). The NOE-derived distance restraints were given upper bounds of 3.0, 4.0, 5.0, and 6.0 Å based upon measured NOE intensities. From an analysis of amide exchange rates measured from a series of $^{15}N/^{1}H$-HSQC spectra recorded after the addition of D_2O, 46 hydrogen bonds for the α-helices were included in the structural calculations. In addition, 109 Φ and angular restraints derived from an analysis of C, N, C_α, H_α, and C_β chemical shifts using the TALOS program (Cornilescu et al., 1999) were included in the structural calculations. A square-well potential was employed to constrain the NMR-derived distance restraints with F_{NOE} set to 150 and 50 kcal mol^{-1} $Å^{-2}$ during stages of high temperature and slow-cooling torsion angle dynamics and final stage of conjugate gradient minimization, respectively. Force constants of 100 and 200 kcal mol^{-1} rad^{-2} were applied to all torsional restraints during the stage of high temperature torsion angle dynamics and the rest stages of structural calculations, respectively.

Quantification of Chemical Shifts

To determine the change in chemical shift upon $Na_v1.2_{IQp}$ binding to apo $CaM_{76\text{-}148}$, or Ca^{2+} binding to apo $CaM_{1\text{-}148}$, net perturbations in both the ^{1}H and ^{15}N dimensions were quantified using the modified Pythagorean theorem in Equation 2.

$$\Delta\delta\ (\text{ppm}) = \left[\left(\Delta^{1}H\,(800.224\ Hz/ppm) \right)^{2} + \left(\Delta^{15}N\,(81.095\ Hz/ppm) \right)^{2} \right]^{1/2} \quad (2)$$

Here, Δδ refers to the linear displacement of a specific resonance peak from its initial position in the reference spectrum.

CaM Binding to $Na_v1.2_{IQp}$

Binding of CaM to Fl-$Na_v1.2_{IQp}$ (50 mM HEPES, 1 mM $MgCl_2$, 5 mM NTA, 50 μM EGTA, pH 7.4) was monitored by fluorescence anisotropy at 22 °C using a Fluorolog 3 (Jobin Yvon, Horiba) fluorimeter. A slight excess of CaM was added (reaching a 1.2:1 ratio of CaM:$Na_v1.2_{IQp}$). The complex was then titrated with a matching buffer that contained 5 M NaCl. Changes in the anisotropy of Fl-$Na_v1.2_{IQp}$ were monitored and analyzed numerically as described previously (Theoharis et al., 2008).

Accession Numbers

The coordinates for this structure were deposited in May, 2010 with the PDB code of 2KXW. A preliminary report of this structure was presented at the 2010 Annual Biophysical Meeting (Feldkamp, Yu, and Shea, 2010).

Note Added in Proof

During revision of this article, Chagot and Chazin deposited and reported a structure (2L53) of apo CaM_{1-148} bound to a peptide representing the IQ motif of NaV1.5 (E1901-L1927) with a short N-terminal tag (GPGS) (Chagot and Chazin, 2011). Superposition of 2KXW and 2L53 using pairs of 68 Cα atoms located in the well defined secondary structure elements showed a RMSD of 1.2 Å. In both 2KXW and 2L53, the apo C-domain adopts the semi-open tertiary conformation. The peptides bound in the same orientation and location despite differences in their sequences. The IQ residues in both peptides interact with almost identical sets of residues on CaM. Slight differences are observed in the two calcium binding loops which are very mobile in the absence of bound calcium. The orientation of the sidechain of Y1916 in our structure is different from that of the corresponding residue F1912 in 2L53, probably reflecting the slight differences in the sequences of both CaM and peptides used in these studies.

Supplementary Material

Refer to Web version on PubMed Central for supplementary material.

Acknowledgments

Supported by the National Institutes of Health RO1 GM 57001 to M.A.S., and by the Roy J. Carver Charitable Trust Grant 01-224.

Abbreviations

NOE Nuclear Overhauser effect

REFERENCES

Ataman ZA, Gakhar L, Sorensen BR, Hell JW, Shea MA. The NMDA Receptor NR1 C1 Region Bound to Calmodulin: Structural Insights into Functional Differences between Homologous Domains. Structure. 2007; 15:1603–1617. [PubMed: 18073110]

Bai Y, Milne JS, Mayne L, Englander SW. Primary structure effects on peptide group hydrogen exchange. Proteins. 1993; 17:75–86. [PubMed: 8234246]

Biswas S, Deschenes I, Disilvestre D, Tian Y, Halperin VL, Tomaselli GF. Calmodulin regulation of Nav1.4 current: role of binding to the carboxyl terminus. J Gen Physiol. 2008; 131:197–209. [PubMed: 18270170]

Brunger AT, Adams PD, Clore GM, DeLano WL, Gros P, Grosse-Kunstleve RW, Jiang JS, Kuszewski J, Nilges N, Pannu NS, et al. Crystallography & NMR system: A new software suite for macromolecular structure determination. Acta Crystallogr. 1998; D54(Pt 5):905–921.

Burgering M, Boelens R, Kaptein R. Observation of intersubunit NOEs in a dimeric P22 Mnt repressor mutant by a time-shared [^{15}N,^{13}C] double half-filter technique. J. Biomol. NMR. 1993; 3:709–714.

Catterall AC. Structure and regulation of voltage-gated Ca^{2+}-channels. Annu.Rev.Cell Dev.Biol. 2000; 16:521–555. [PubMed: 11031246]

Chagot B, Chazin WJ. Solution NMR Structure of Apo-Calmodulin in Complex with the IQ Motif of Human Cardiac Sodium Channel $Na_V1.5$. Journal of Molecular Biology. 2011; 406:106–119. [PubMed: 21167176]

Clore GM, Gronenborn AM. Multidimensional heteronuclear magnetic resonance of proteins. Meths. Enzymol. 1994; 239:349–363.

Cormier JW, Rivolta I, Tateyama M, Yang AS, Kass RS. Secondary Structure of the Human Cardiac Na^+ Channel C Terminus. Journal of Biological Chemistry. 2002; 277:9233–9241. [PubMed: 11741959]

Cornilescu G, Delaglio F, Bax A. Protein backbone angle restraints from searching a database for chemical shift and sequence homology. J Biomol NMR. 1999; 13:289–302. [PubMed: 10212987]

Crivici A, Ikura M. Molecular and Structural Basis of Target Recognition by Calmodulin. Annual Review of Biophysics and Biomolecular Structure. 1995; 24:85–116.

Delaglio F, Grzesiek S, Vuister GW, Zhu G, Pfeifer J, Bax A. NMRPipe: a multidimensional spectral processing system based on UNIX pipes. J Biomol NMR. 1995; 6:277–293. [PubMed: 8520220]

DeMaria CD, Soong TW, Alseikhan BA, Alvania RS, Yue DT. Calmodulin bifurcates the local Ca^{2+} signal that modulates P/Q-type Ca^{2+} channels. Nature. 2001; 411:484–489. [PubMed: 11373682]

Drum CL, Yan S, Bard J, Shen Y, LU D, Soelaiman S, Grabarek Z, Bohm A, Tang W. Structural basis for the activation of anthrax adenylyl cyclase exotoxin by calmodulin. Nature. 2002; 415:396–402. [PubMed: 11807546]

Feldkamp MD, Yu L, Shea MA. Calmodulin Regulation of the Neuronal Voltage-Dependent Sodium Channel. Biophysical Journal. 2010; 98:310a.

Fesik SW, Zuiderweg ERP. Heteronuclear three-dimensional NMR spectroscopy. A strategy for the simplification of homonuclear two-dimensional NMR spectra. J. Magn. Reson. 1988; 78:588–593.

Fraczkiewicz R, Braun W. Exact and Efficient Analytical Calculation of the Accessible Surface Areas and Their Gradients for Macromolecules. J. Comp. Chem. 1998; 19:319–333.

Gemmecker G, Olejniczak ET, Fesik SW. An improved method for selectively observing protons attached to 12C in the presence of ^{1}H-^{13}C spin pairs. J. Magn. Reson. 1992; 96:199–204.

Goddard, TD.; Kneller, DG. SPARKY. University of California; San Francisco:

Houdusse A, Gaucher JF, Krementsova E, Mui S, Trybus KM, Cohen C. Crystal structure of apo-calmodulin bound to the first two IQ motifs of myosin V reveals essential recognition features. Proc Natl Acad Sci U S A. 2006; 103:19326–19331. [PubMed: 17151196]

Ikura M, Bax A. Isotope-filtered 2D NMR of a protein-peptide complex: study of a skeletal muscle myosin light chain kinase fragment bound to calmodulin. J. Am. Chem. Soc. 1992; 114:2433–2440.

Kim EY, Rumpf CH, Fujiwara Y, Cooley ES, Van Petegem F, Minor DL Jr. Structures of CaV2 Ca^{2+}/CaM-IQ domain complexes reveal binding modes that underlie calcium-dependent inactivation and facilitation. Structure. 2008; 16:1455–1467. [PubMed: 18940602]

Klee, CB.; Newton, DL.; Ni, WC.; Haiech, J. Regulation of the calcium signal by calmodulin. In: Evered, D.; Whelan, J., editors. Calcium and the Cell. John Wiley & Sons; Chichester, New York: 1986. p. 162-182.

Kung C, Preston RR, Maley ME, Ling K-Y, Kanabrocki JA, Seavey BR, Saimi Y. *In vivo Paramecium* mutants show that calmodulin orchestrates membrane responses to stimuli. Cell Calcium. 1992; 13:413–425. [PubMed: 1380404]

Liu Y, Storm DR. Regulation of free calmodulin levels by neuromodulin: Neuron growth and regeneration. TIPS. 1990; 11:107–111. [PubMed: 2151780]

Mantegazza M, Yu FH, Catterall WA, Scheuer T. Role of the C-terminal domain in inactivation of brain and cardiac sodium channel. Proceedings of the National Academy of Science. 2001; 98:15348–15353.

Molday RS, Englander SW, Kallen RG. Primary structure effects on peptide group hydrogen exchange. Biochemistry. 1972; 11:150–158. [PubMed: 5061873]

Mori M, Konno T, Ozawa T, Murata M, Imoto K, Nagayama K. Novel Interaction of the Voltage-Dependent Sodium Channel (VDSC) with Calmodulin: Does VDSC Acquire Calmodulin-Mediated Ca^{2+}-Sensitivity? Biochemistry. 2000; 39:1316–1323. [PubMed: 10684611]

Mori MX, Kooi C.W. Vander, Leahy DJ, Yue DT. Crystal structure of the CaV2 IQ domain in complex with Ca^{2+}/calmodulin: high-resolution mechanistic implications for channel regulation by Ca^{2+} Structure. 2008; 16:607–620. [PubMed: 18400181]

Newman RA, Van Scyoc WS, Sorensen BR, Jaren OR, Shea MA. Interdomain cooperativity of calmodulin to melittin preferentially increases calcium affinity of sites I and II. Proteins: Structure, Function, and Bioinformatics. 2008; 71:1792–1812.

Otting G, Wuthrich K. Extended heteronuclear editing of 2D ^{1}H NMR spectra of isotope-labeled proteins, using the X(omega1, omega2) double half filter. J. Magn. Reson. 1989; 85:586–594.

Pettersen EF, Goddard TD, Huang CC, Couch GS, Greenblatt DM, Meng EC, Ferrin TE. UCSF Chimera--a visualization system for exploratory research and analysis. J Comput Chem. 2004; 25:1605–1612. [PubMed: 15264254]

Putkey JA, Slaughter GR, Means AR. Bacterial expression and characterization of proteins derived from the chicken calmodulin cDNA and a calmodulin processed gene. Journal of Biological Chemistry. 1985; 260:4704–4712. [PubMed: 2985564]

Sarhan MF, Van Petegem F, Ahern CA. A double tyrosine motif in the cardiac sodium channel domain III-IV linker couples calcium-dependent calmodulin binding to inactivation gating. J Biol Chem. 2009; 284:33265–33274. [PubMed: 19808664]

Schaller KL, Caldwell JH. Expression and distribution of voltage-gated sodium channels in the cerebellum. Cerebellum. 2003; 2:2–9. [PubMed: 12882229]

Schumacher MA, Rivard AF, Bachinger HP, Adelman JP. Structure of the gating domain of a Ca^{2+}-activated K^{+} channel complexed with Ca^{2+}/calmodulin. Nature. 2001; 410:1120–1124. [PubMed: 11323678]

Shah VN, Wingo TL, Weiss KL, Williams CK, Balser JR, Chazin WJ. Calcium-dependent regulation of the voltage-gated sodium channel hH1: intrinsic and extrinsic sensors use a common molecular switch. Proc Natl Acad Sci U S A. 2006; 103:3592–3597. [PubMed: 16505387]

Sobolev V, Sorokine A, Prilusky J, Abola EE, Edelman M. Automated analysis of interatomic contacts in proteins. Bioinformatics. 1999; 15:327–332. [PubMed: 10320401]

Stein EG, Rice LM, Brünger AT. Torsion-Angle Molecular Dynamics as a New Efficient Tool for NMR Structure Calculation. J. Magn. Reson. 1997; 124:154–164. [PubMed: 9424305]

Swindells MB, Ikura M. Pre-formation of the semi-open conformation by the apo-calmodulin C-terminal domain and implications for binding IQ-motifs. Nature Structural Biology. 1996; 3:501–504.

Terrak M, Wu G, Stafford WF, Lu RC, Dominguez R. Two distinct myosin light chain structures are induced by specific variations within the bound IQ motifs - functional implications. European Molecular Biology Organization Journal. 2003; 22:362–371.

Theoharis NT, Sorensen BR, Theisen-Toupal J, Shea MA. The Neuronal Voltage-Dependent Sodium Channel Type II IQ Motif Lowers the Calcium Affinity of the C-Domain of Calmodulin. Biochemistry. 2008; 47:112–123. [PubMed: 18067319]

Urbauer JL, Short JH, Dow LK, Wand AJ. Structural Analysis of a Novel Interaction by Calmodulin: High Affinity Binding of a Peptide in the Absence of Calcium. Biochemistry. 1995; 34:8099–8109. [PubMed: 7794923]

Venosa RA. Inward movement of sodium ions in resting and stimulated frog′s sartorius muscle. J Physiol. 1974; 241:155–173. [PubMed: 4547580]

Weiss LA, Escayg A, Kearney JA, Trudeau M, MacDonald BT, Mori M, Reichert J, Buxbaum JD, Meisler MH. Sodium channels SCN1A, SCN2A and SCN3A in familial autism. Molecular Psychistry. 2003; 8:186–194.

Yamazaki T, Lee W, Arrowsmith CH, Muhandiram DR, Kay LE. A suite of triple-resonance NMR experiments for the backbone assignment of ^{15}N, ^{13}C, ^{2}H-labeled proteins with high sensitivity. J. Am. Chem. Soc. 1994; 116:11655–11666.

Yap KL, Kim J, Truong K, Sherman M, Yuan T, Ikura M. Calmodulin Target Database. Journal of Structural and Functional Genomics. 2000; 1:8–14. [PubMed: 12836676]

Yu FH, Catterall WA. Overview of the voltage-gated sodium channel family. Genome Biology. 2003; 4:207.201–207.207. [PubMed: 12620097]

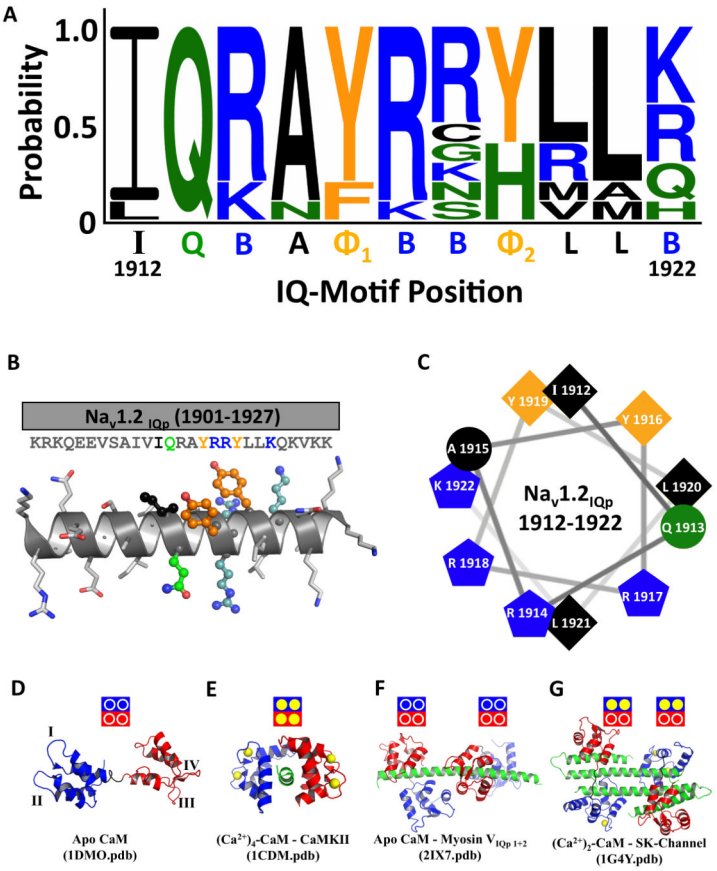

Figure 1. Features of Voltage-Dependent Sodium Channel IQ Motifs and CaM

A: Consensus sequence of 10 human voltage-dependent sodium channel IQ motifs. **B:** $Na_v1.2_{IQp}$ sequence modeled as an ideal α-helix. **C**: Helical wheel projection of IQ motif of $Na_v1.2_{IQp}$ displaying its hydrophobic and polar faces. **D-G**: Four structures of CaM (residues 1-75 blue, 76-80 black, 81-148 red) shown with bound peptide (green) and Ca^{2+} (yellow spheres) as appropriate. Square icons above ribbon diagrams indicate apo (open circle) or Ca^{2+}-saturated (yellow filled circle) sites in the N-domain (blue) and C-domain (red).

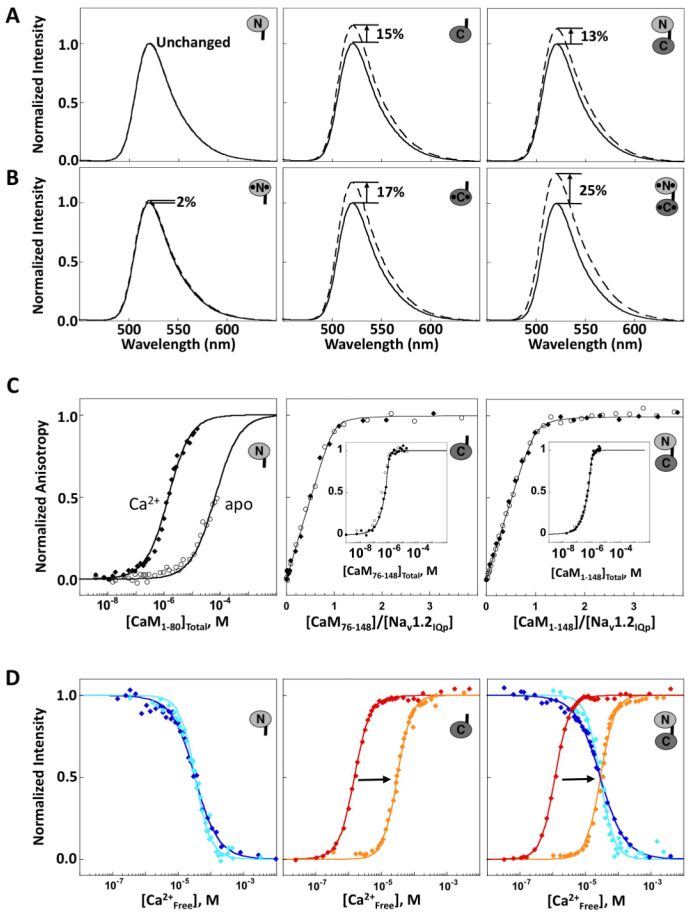

Figure 2. Domain-specific Interactions of CaM with $Na_V1.2_{IQp}$

Emission spectra of Fl-$Na_V1.2_{IQp}$ in the absence (solid line) and presence (dashed line) of slight excess of (**A**) apo CaM_{1-80} (left), apo CaM_{76-148} (middle), and apo CaM_{1-148} (right) or (**B**) Ca^{2+}-saturated CaM. **C:** Titration of Fl-$Na_V1.2_{IQp}$ with apo CaM (open circles) or Ca^{2+}-saturated CaM (filled diamonds). The titrations of apo CaM_{1-80} were normalized to the maximum signal observed after addition of 10 mM $CaCl_2$ (Newman, 2008). For CaM_{76-148} (middle), and CaM_{1-148} (right), binding was stoichiometric and is plotted as a function of the ratio of [CaM_{total}]:[peptide], with an inset showing saturation versus [CaM_{total}]. **D:** Equilibrium Ca^{2+} titrations of CaM_{1-80} (left), CaM_{76-148} (middle), and CaM_{1-148} (right) using intrinsic fluorescence to monitor Ca^{2+} binding in the absence of peptide [sites I and II (blue) or sites III and IV (red)], or after addition of excess $Na_V1.2_{IQp}$ [sites I and II (cyan) and sites III and IV (orange)]. Supported by Tables S1 and S2.

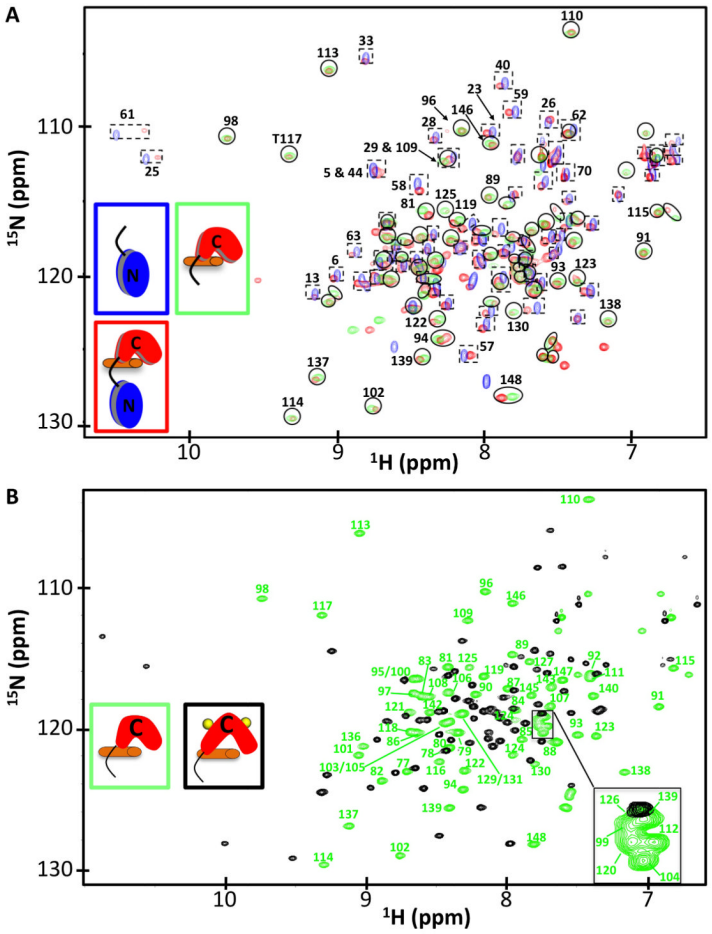

Figure 3. 15N/^{1}H-HSQC Spectra of ^{13}C,^{15}N-CaM

A: Overlapping peaks in ^{15}N/^{1}H-HSQC spectra of apo $CaM_{1\text{-}80}$ (blue) and apo $CaM_{1\text{-}148}$ with equimolar $Na_v1.2_{IQp}$ (red) are boxed by dashed squares, while those overlapped in the apo $CaM_{76\text{-}148}$ (green) and apo $CaM_{1\text{-}148}$ with equimolar $Na_v1.2_{IQp}$ (red) are shown by solid circles. The spectra of apo $CaM_{1\text{-}80}$ alone and apo $CaM_{76\text{-}148}$:$Na_v1.2_{IQp}$ complex account for > 95% of the peaks of apo $CaM_{1\text{-}148}$-$Na_v1.2_{IQp}$ **B:** Overlay of ^{15}N/^{1}H-HSQC spectra of apo $CaM_{76\text{-}148}$ (green) and $(Ca^{2+})_2$-$CaM_{76\text{-}148}$ (black), each with equimolar $Na_v1.2_{IQp}$. Cross peaks of apo $CaM_{76\text{-}148}$-$Na_v1.2_{IQp}$ are labeled. Supported by Figures S1, S2, S3.

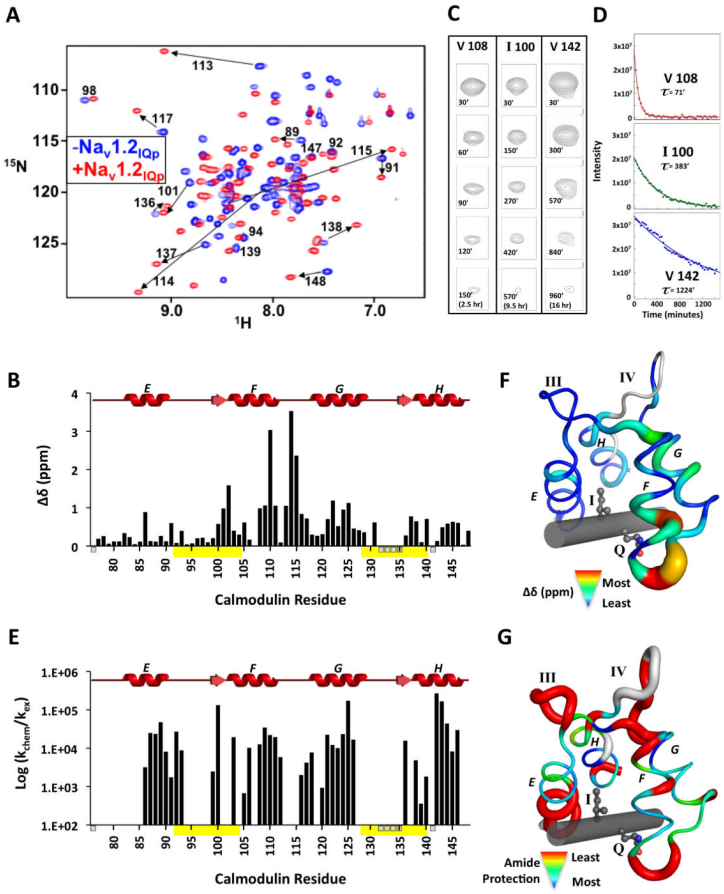

Figure 4. 15N/^{1}H-HSQC-Detected Changes in Apo CaM$_{76-148}$ upon Na$_v$1.2$_{IQp}$ Addition

A: Overlay of ^{15}N/^{1}H-HSQC spectra of apo CaM$_{76-148}$ (blue) and apo CaM$_{76-148}$ bound to Na$_v$1.2$_{IQp}$ (red). **B:** Quantified backbone amide chemical shift perturbations of apo CaM$_{76-148}$ upon binding Na$_v$1.2$_{Iqp}$. Ca^{2+}-binding sites are yellow bars. Unassigned residues (76, 132, 133, 134, 135, 141) are indicated as small bars below the abscissa. **C:** ^{15}N/^{1}H-HSQC crosspeak intensities at identical contour levels showing residues of apo CaM$_{76-148}$ bound to Na$_v$1.2$_{IQp}$. **D:** Fitted exchange curves and rates for the residues shown in C. **E:** Bar graph of amide protection factors. Chemical shift perturbations (**F**) and protection factor magnitudes (**G**) mapped onto the structure of apo CaM$_{76-148}$:Na$_v$1.2$_{IQp}$ (unassigned residues are light gray; Na$_v$1.2$_{IQp}$ is a gray rod). Supported by Table S3.

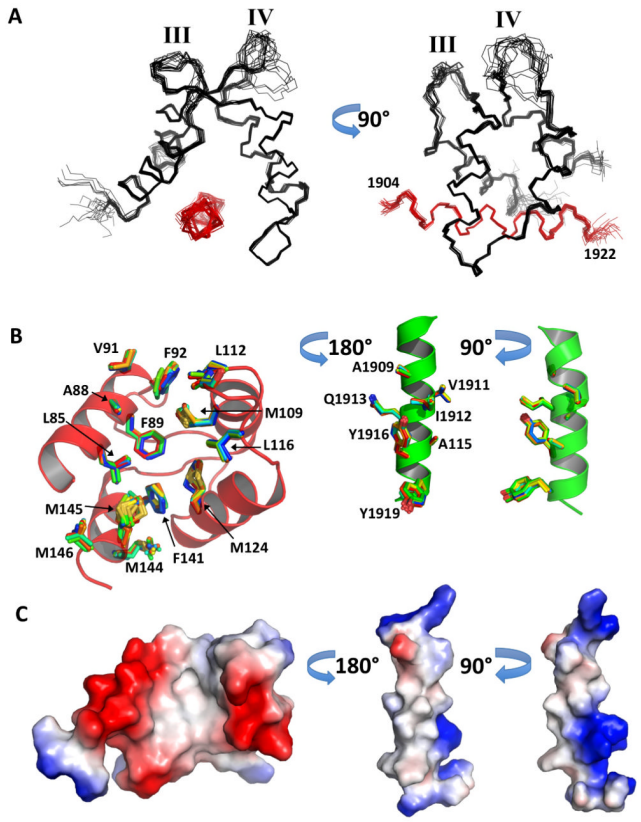

Figure 5. Solution Structure of Apo $CaM_{76\text{-}148}$:$Na_v1.2_{IQp}$

A: Ensemble of 20 lowest energy structures of apo $CaM_{76\text{-}148}$ (black) bound to $Na_v1.2_{IQp}$ (red) **B:** Hydrophobic interaction interfaces of 20 lowest energy structures in 2KXW. Apo $CaM_{76\text{-}148}$ and residues 1904-1922 of $Na_v1.2_{IQp}$ (green backbone) with selected interfacial hydrophobic residues shown in sticks. **C:** Vacuum electrostatic potentials mapped on the surface apo $CaM_{76\text{-}148}$ and $Na_v1.2_{IQp}$. Surfaces are positive (blue), negative (red) or hydrophobic (white). Supported by Figure S4 and Movies S1 and S2.

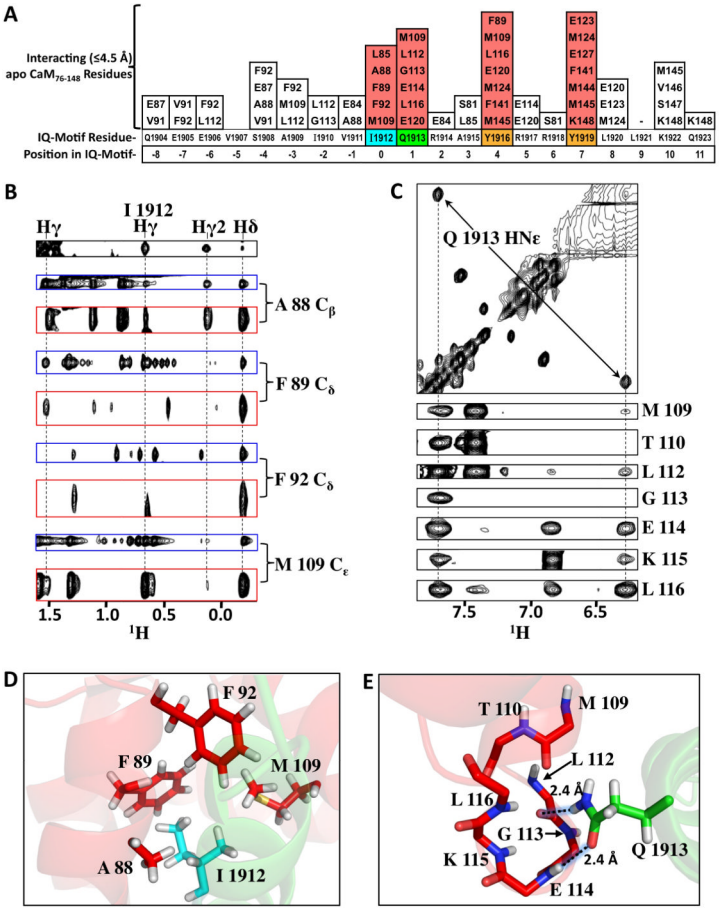

Figure 6. Analysis of apo CaM_{76-148}:$Na_V1.2_{IQp}$ Binding Interface

A: Residues of apo CaM_{76-148} within 4.5 Å of each residue of $Na_V1.2_{IQp}$ in 2KXW are listed; four peptide residues (I1912, Q1913, Y1916, Y1919) made • 5 contacts (highlighted in red). 5 contacts (highlighted in red). **B:** Slices of NOESY spectra showing intermolecular NOEs observed between I1912 of $Na_V1.2_{IQp}$ and apo CaM_{76-148}. Slices from the 3D ^{13}C-edited NOESY spectra are in blue boxes, while slices from 3D ^{13}C-edited and ^{12}C,^{14}N-filtered NOESY spectrum are in red boxes. **C:** Top panel shows Q1913 carboxamide proton shifts in the 2D ^{12}C,^{14}N-filtered NOESY spectrum, and lower panels show slices of ^{15}N-edited NOESY spectra showing NOEs between $Na_V1.2_{IQp}$ Q1913 $N_\varepsilon H_2$ and 7 loop backbone amides in apo CaM_{76-148}. **D:** Location of apo CaM_{76-148} residues shown in panel B relative to I1912. **E:** Location of apo CaM_{76-148} residues shown in panel C relative to Q1913. Dashed lines show hydrogen bonds between the carboxamide of Q1913 and backbone atoms of L112 and E114.

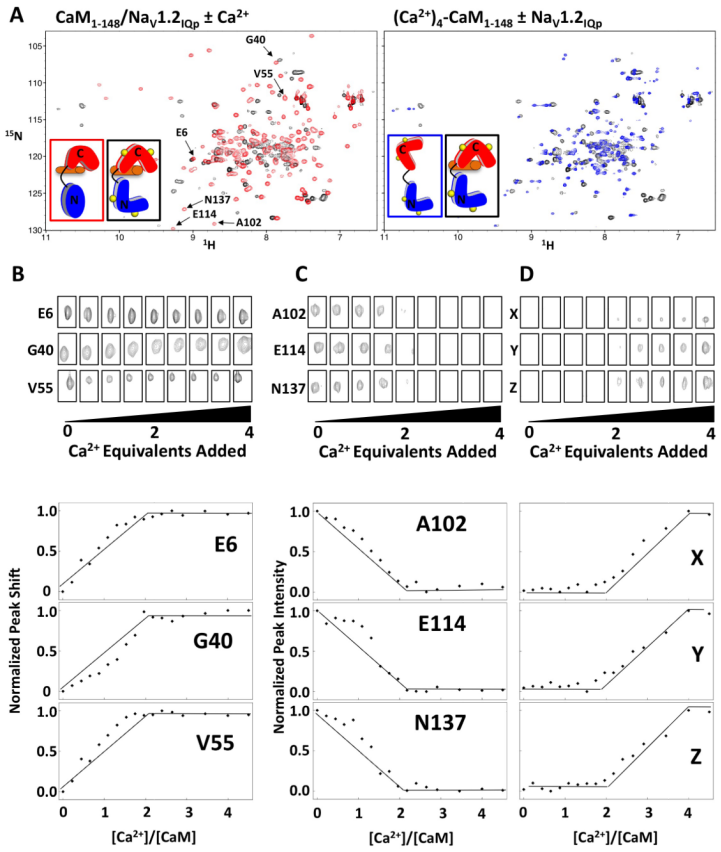

Figure 7. Ca^{2+} binding to Apo CaM_{1-148}:$Na_V1.2_{IQp}$

A: $^{15}N/^{1}H$-HSQC spectral overlays of apo (red) and $(Ca^{2+})_4$-CaM_{1-148} (black) when bound to $Na_V1.2_{IQp}$ (left panel) and $(Ca^{2+})_4$-CaM_{1-148} alone (blue) and bound (black) to $Na_V1.2_{IQp}$ (right panel). B: $^{15}N/^{1}H$-HSQC cross peak intensity and position as a function of added Ca^{2+} equivalents for selected N-domain residues (E6, G40, V55) of apo CaM_{1-148}, selected C-domain residues (A102, E114, N137) of CaM_{1-148}, and three unassigned C-domain residues (X, Y, Z) of CaM_{1-148} when Ca^{2+}-saturated. The quantified change in chemical shift perturbations as a function of added Ca^{2+} equivalents for these residues are plotted in the lower panels. Supported by Figure S6.

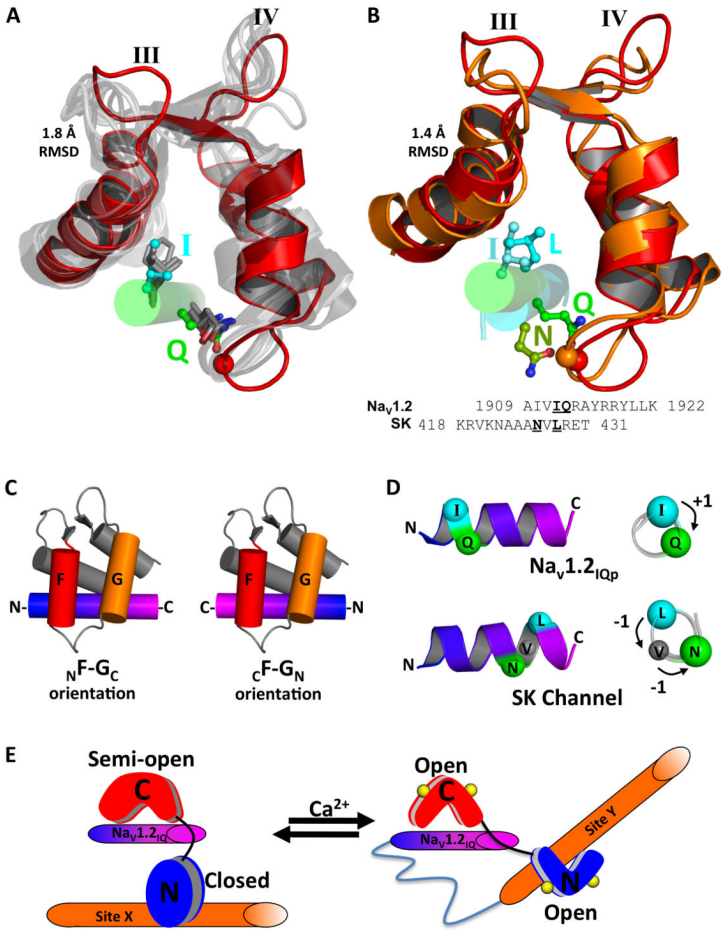

Figure 8. Conserved Features of Apo Semi-Open EF-Hand Domains and Model for CaM:Na$_V$1.2 Binding to Recognition Motifs

A: Structural comparison of apo CaM$_{76\text{-}148}$ (red):Na$_v$1.2$_{IQp}$ (green rod) complex (2KXW) with the C-domains of apo CaM and apo CaM-like proteins (gray) bound to canonical IQ motifs (2IX7, 1M45, 1M46, 1ND2, and 3JVT). I and Q residues of all IQ motifs are sticks; C_α of residue 113 of CaM is a red sphere. **B:** Structural comparison of apo CaM$_{76\text{-}148}$ (red):Na$_v$1.2$_{IQp}$ (green rod) complex with the apo C-domain of $(Ca^{2+})_2$-CaM$_{1\text{-}148}$ (orange) bound to SK$_p$ (cyan). I1912 and Q1913 (Na$_v$1.2$_{IQp}$) and L428 and N426 (SK$_p$) are ball-and-stick; CaM residue 113 shown as red or orange sphere. Sequences of Na$_v$1.2$_{IQp}$ and SK$_p$ are aligned structurally based on the hydrophobic interaction of I1912 and L428 and carboxamide-containing Q1913 and N426. **C:** Two alternative polarities for peptides binding to the C-domain of CaM; $_N$F-G$_C$ depicts the N-terminus (blue) closest to helix F (red), while $_C$F-G$_N$ depicts the C-terminus (magenta) closest to helix F and farthest from helix G (orange). **D:** Relative positions of the hydrophobic (cyan spheres) and carboxamide (green spheres) residues. The blue-to-magenta color gradient indicates $_N$F-G$_C$ polarity. **E:** Proposed model of CaM$_{1\text{-}148}$ interacting with Na$_v$1.2. The IQ motif interacts solely with the semi-open C-domain of CaM. The N-domain is in a closed conformation that may interact with an unidentified site X elsewhere on Na$_v$1.2. Under Ca^{2+}-saturating conditions, the C-domain remains bound to Na$_v$1.2$_{IQp}$; the open N-domain may bind to site Y (potentially distinct from site X). Supported by Figure S6.

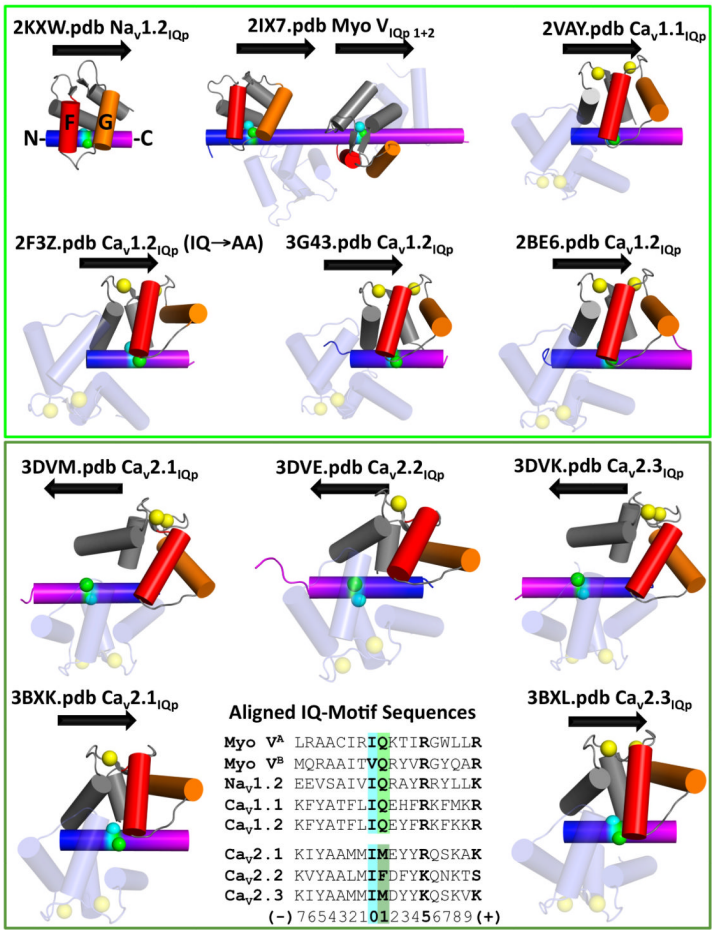

Figure 9. Orientation of Canonical and Non-Canonical IQ Motifs Bound to CaM

CaM is bound to peptides containing canonical (upper panel) or non-canonical (lower panel) IQ motifs. Each ribbon diagram is labeled with PDB ID and degree of Ca^{2+} binding (yellow spheres). In CaM, helix F is red, and G is orange. Helical polarity of each IQ motif is indicated by a color gradient from N- (blue) to C-terminus (magenta) and corresponding arrow. Residues at positions 0 (cyan) and 1 (green) are indicated by spheres. In the lower panel, sequences of binding motifs are aligned according to positions 0 and 1.

Table 1

Structural statistics and root-mean-square deviation for 20 structures of apo $CaM_{76\text{-}148}$:$Na_v1.2_{IQp}$ complex

Structural statistics[a]	<SA>	$\langle \bar{SA} \rangle_r$
RMSD from experimental distance restraints (Å)[b]		
All (1865)	0.008 ± 0.001	0.007
CaM intra-residue (457)	0.007 ± 0.002	0.005
CaM sequential (298)	0.005 ± 0.004	0.003
CaM medium range (300)	0.009 ± 0.002	0.008
CaM long range (331)	0.006 ± 0.001	0.005
Intra-peptide (245)	0.005 ± 0.002	0.003
CaM-peptide intermolecular (188)	0.012 ± 0.002	0.011
hydrogen bond (46)	0.016 ± 0.001	0.021
RMSD from experimental torsional angle restraints (deg)[c]		
Φ and Ψ angles (109)	0.3 ± 0.03	0.2
Ramachandran Statistics[d]		
Residues in most favored regions	80.2%	
Residues in additional allowed regions	17.6%	
Residues in generously allowed regions	2.2%	
Residues in disallowed regions	0.0%	
CNS Potential Energy (kcal/mol)		
E_{tot}	89 ± 4.8	80
E_{bond}	5 ± 0.5	1
E_{ang}	65 ± 2.9	62
E_{imp}	5 ± 0.6	4
E_{repel}	6 ± 1.2	6
E_{noe}	6 ± 1.2	5
E_{cdih}	1 ± 0.1	1
Cartesian coordinate RMSD (Å)	N, C_a, and C’	all heavy
<SA> vs. $\langle \bar{SA} \rangle_r$[e]	0.31 ± 0.05	0.95 ± 0.11

[a] Where <SA> is the ensemble of 20 NMR-derived solution structures of CaM/peptide; $\langle \bar{SA} \rangle_r$ is the mean atomic structure; $\langle \bar{SA} \rangle_r$ is the energy-minimized average structure. The CNS F_{repel} function was used to simulate van der Waals interactions using a force constant of 4.0 kcal/mol $Å^{-4}$ with the atomic radii set to 0.8 times their CHARMM values.

[b] Distance restraints were employed with a square-well potential (F_{noe} = 50 kcal/mol $Å^{-2}$). Hydrogen bonds were given bounds of 1.8-2.4 Å (H-O) and 2.7-3.3 Å (N-O). No distance restraint was violated by more than 0.3 Å in any of the final structures.

[c] Torsional restraints were applied with values derived from an analysis of the C’, N, C_a, H_a, and C_b chemical shifts using the TALOS program. Force constant of 200 kcal mol^{-1} rad^{-2} was applied for all torsional restraints.

[d] Ramachandran statistics calculated with ProCheck. http://www.ebi.ac.uk/thornton-srv/software/PROCHECK/

[e] RMSD for CaM residues 80-128 and 134-146 and peptide residues 1905-1920.